

**Photo-induced double-strand DNA and site-specific protein cleavage activity  
of L-histidine ( $\mu$ -oxo)diiron(III) complexes of heterocyclic bases**

Mithun Roy, Tuhin Bhowmick, Ramkumar Santhanagopal, Suryanarayana Ramakumar and  
Akhil R. Chakravarty\*<sup>a</sup>

*Department of Inorganic and Physical Chemistry and Bioinformatics center, Department of  
Physics, Indian Institute of Science, Bangalore 560012, India*

Fax: +91-80-23600683; E-mail: [arc@ipc.iisc.ernet.in](mailto:arc@ipc.iisc.ernet.in)

Electronic Supplementary Information

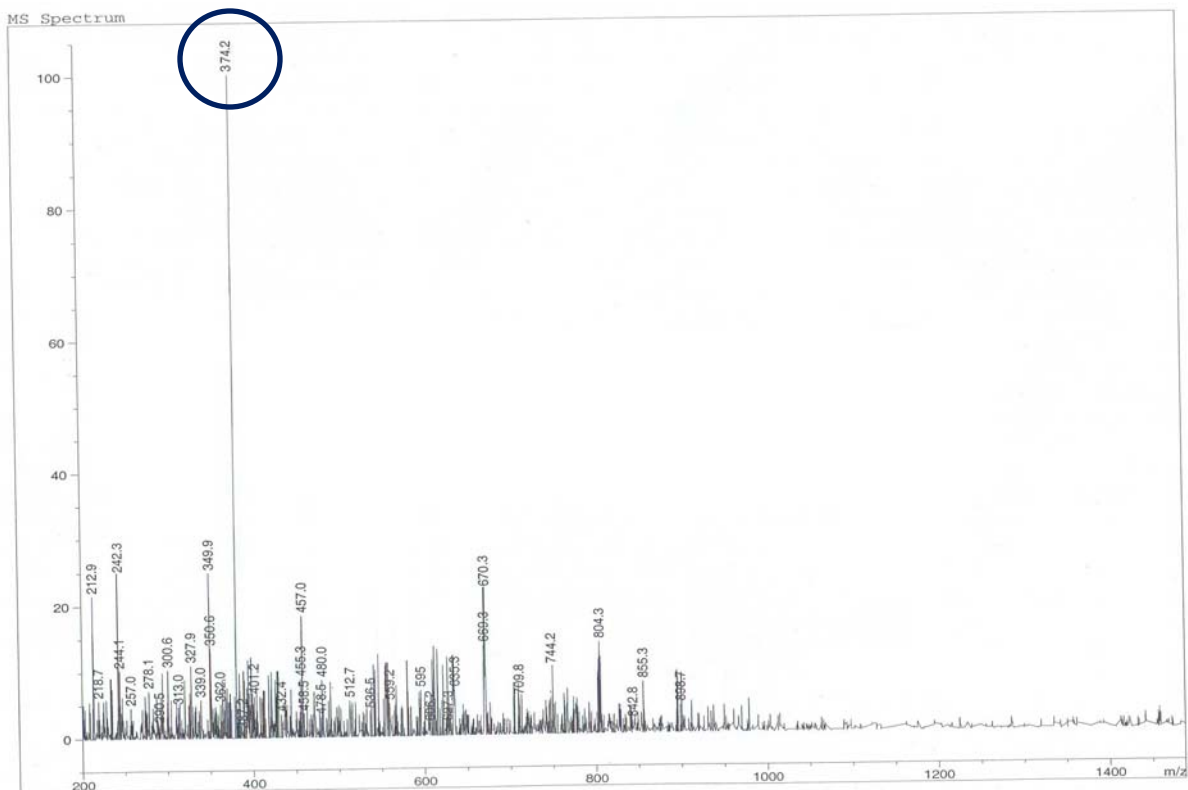


**Fig. S1.** ESI-MS spectrum of complex **1** in H<sub>2</sub>O showing the parent ion peak at m/z 374 [M-2(CIO<sub>4</sub><sup>-</sup>)]<sup>2+</sup>.

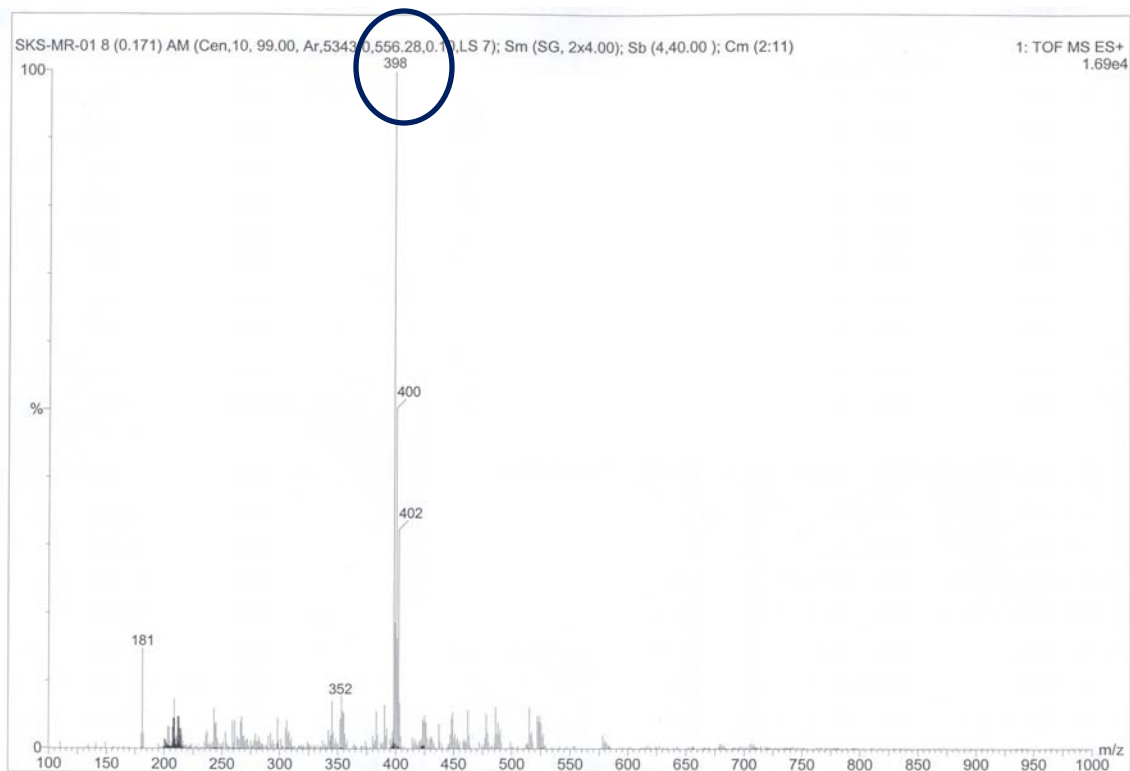


**Fig. S2.** ESI-MS spectrum of complex **2** in H<sub>2</sub>O showing the parent ion peak at m/z 398 [M-2(CIO<sub>4</sub><sup>-</sup>)]<sup>2+</sup>.

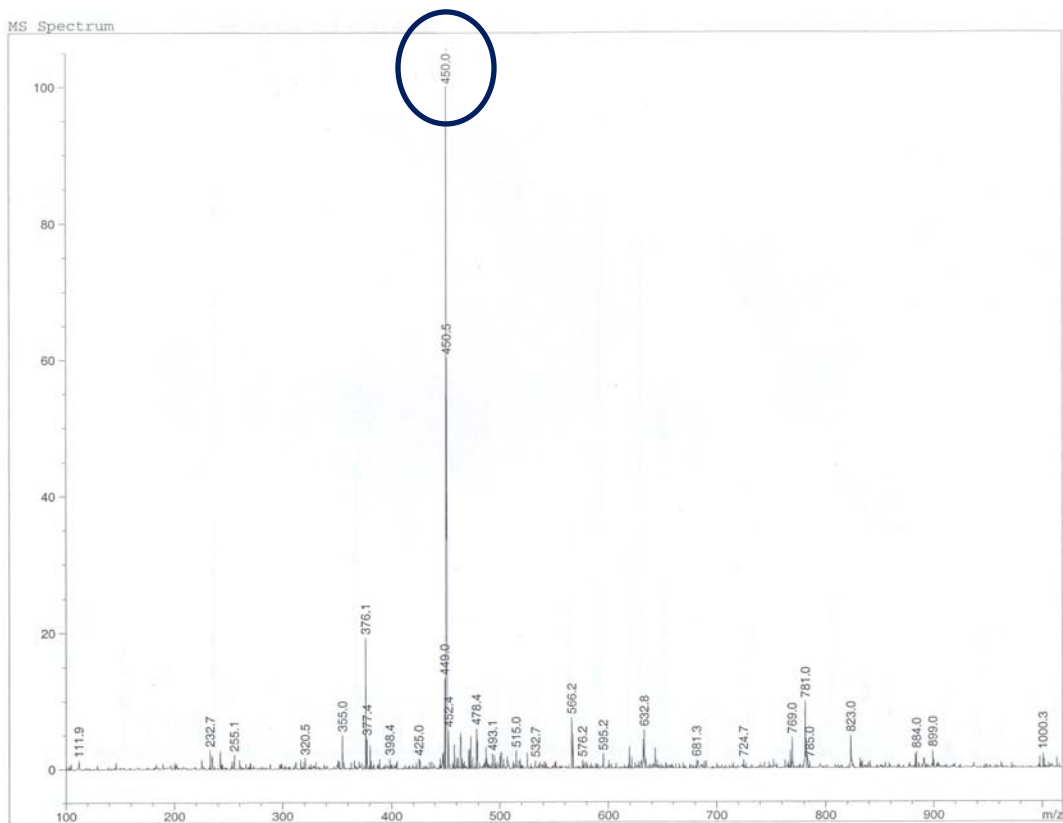


**Fig. S3.** ESI-MS spectrum of complex **3** in H<sub>2</sub>O showing the parent ion peak at  $m/z$  450 [M-2(ClO<sub>4</sub>)]<sup>2+</sup>.

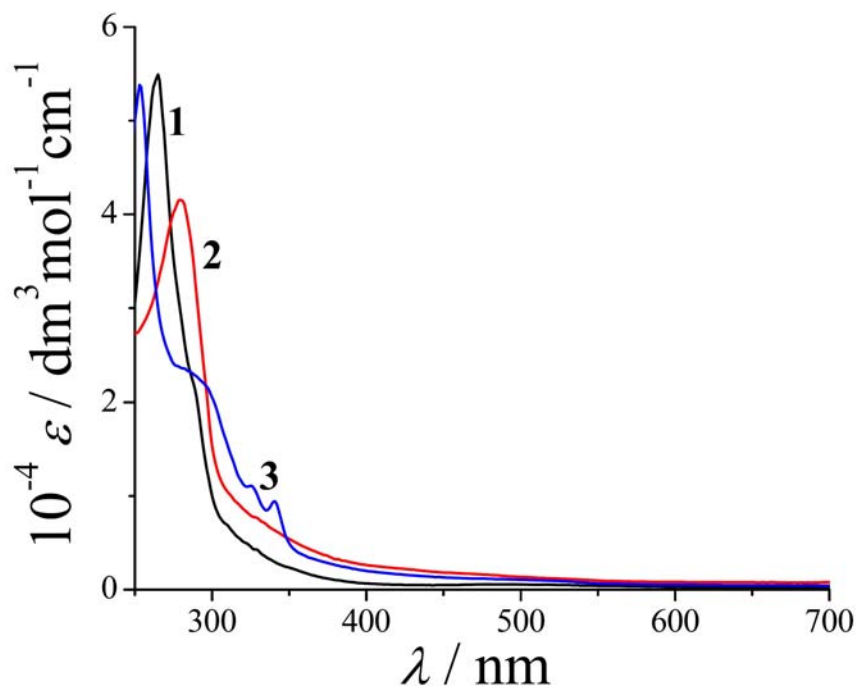


**Fig. S4.** The electronic absorption spectra of the complexes **1**(—), **2**(—) and **3**(—) in Tris-HCl buffer.

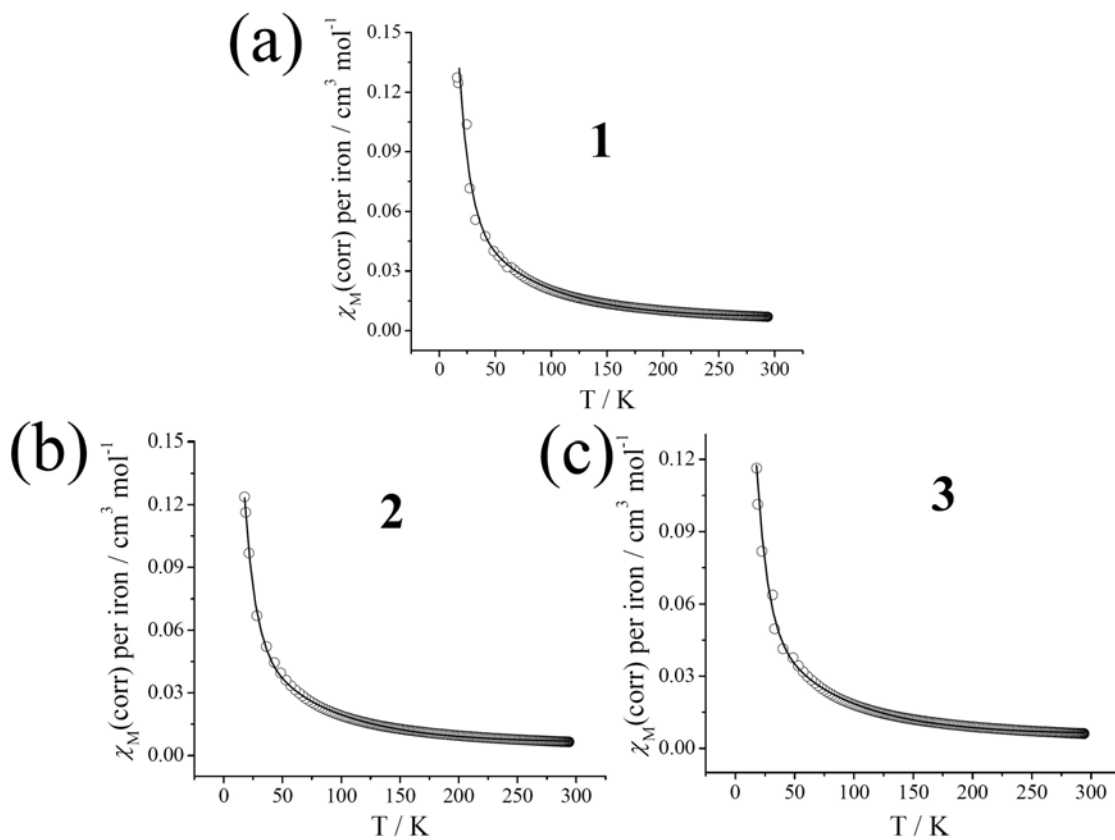


**Fig. S5.** Temperature dependence (295-18 K) of the molar magnetic susceptibility per iron(III) (circle) of the complexes **1** (a), **2** (b) and **3** (c). The solid lines represent the theoretical fits using the equation described in the text.

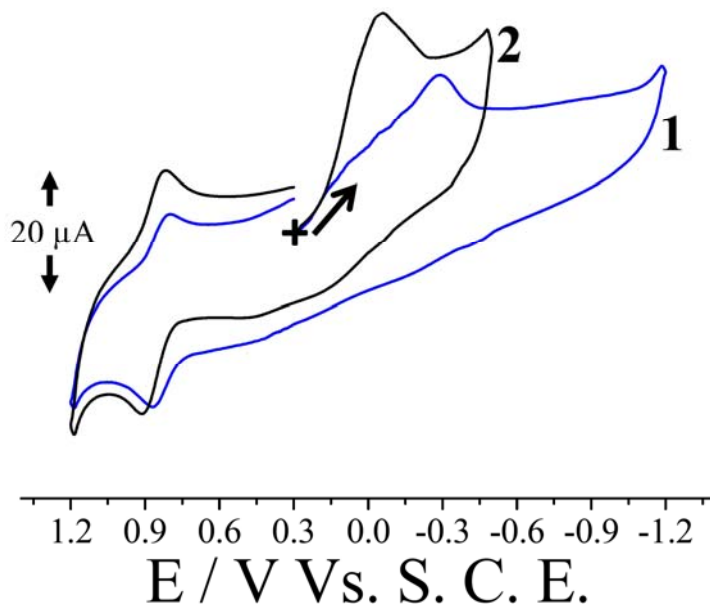


**Fig. S6.** The cyclic voltammetric responses of the complexes **1** (—) and **2** (—) in  $\text{H}_2\text{O}$ -0.1M KCl at a scan rate of  $50 \text{ mV s}^{-1}$  with reference to S.C.E. The reversible voltammogram near 0.85 V is due to the formation of the binary complex of iron(II) from degradation of the diiron species.

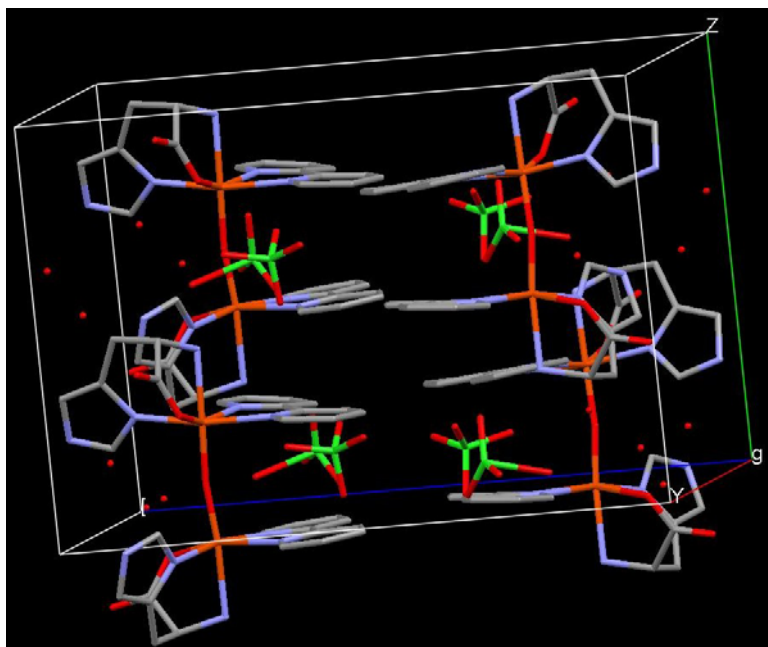


**Fig. S7.** Unit cell packing diagram of the complex  $1 \cdot 4\text{H}_2\text{O}$ .

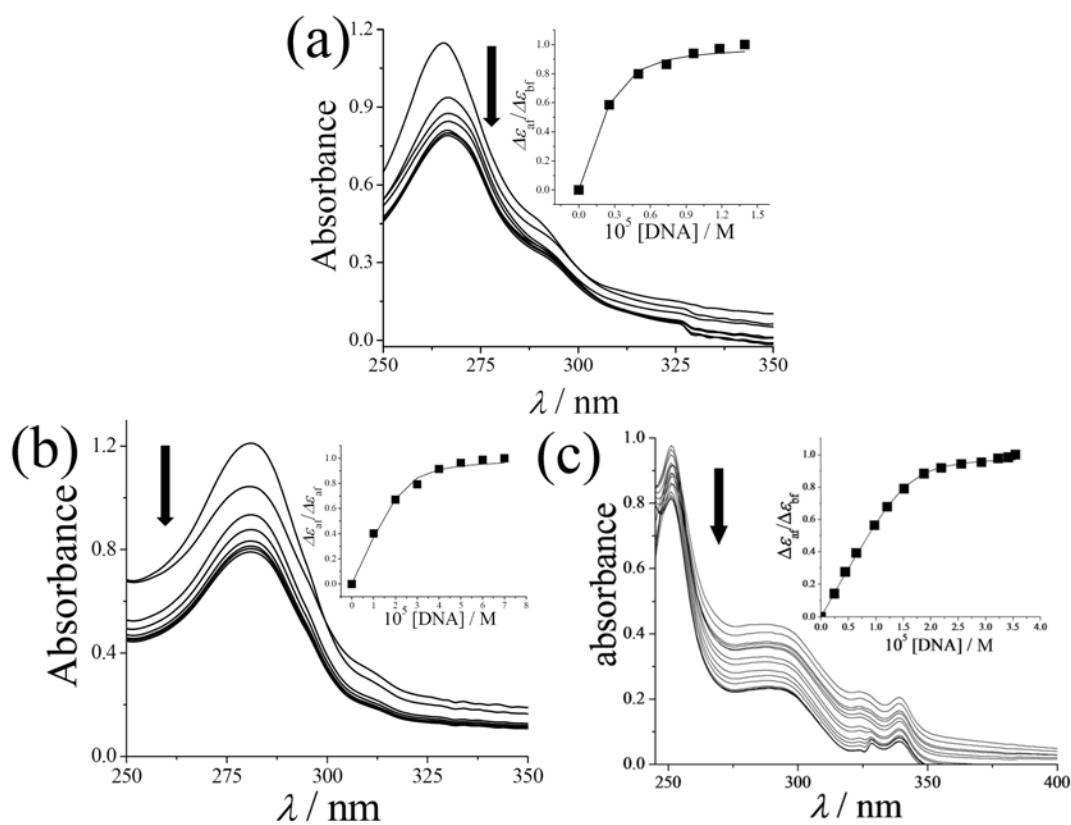


**Fig. S8.** Spectral traces showing the effect of addition of CT DNA ( $130 \mu\text{M}$  NP) to a  $30 \mu\text{M}$  complex **1** (a), **2** (b) and **3** (c) in Tris-HCl buffer (pH 7.2) with the insets showing the MvH plots ( $\Delta\epsilon_{af}/\Delta\epsilon_{bf}$  vs. [DNA]). The experimental details are given in the text.

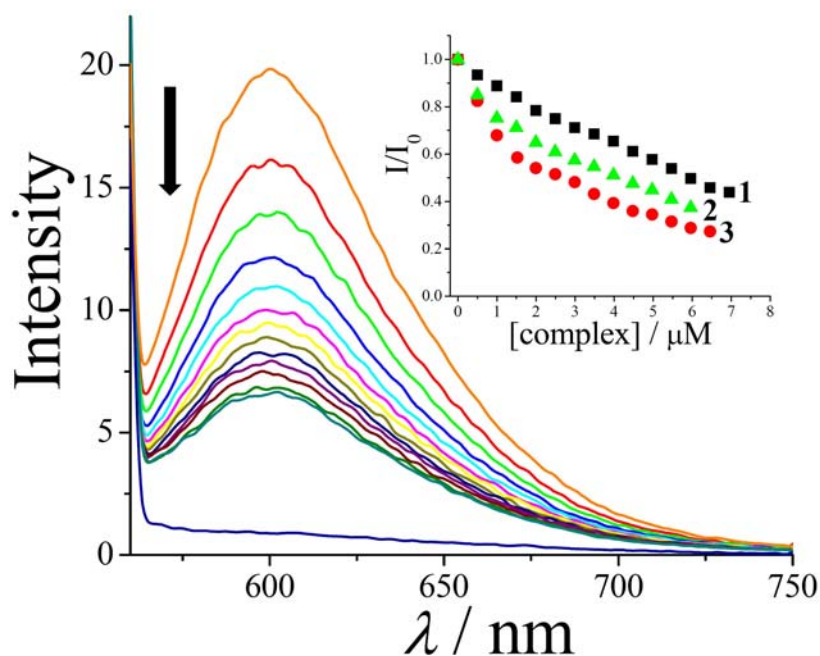


**Fig. S9.** The effect of addition of increasing amount of **3** to an ethidium bromide bound CT DNA in 5 mM Tris-HCl buffer at 25 °C. The inset shows the plots of  $I/I_0$  vs. [complex] (1, ■; 2, ▲ and 3, ●).

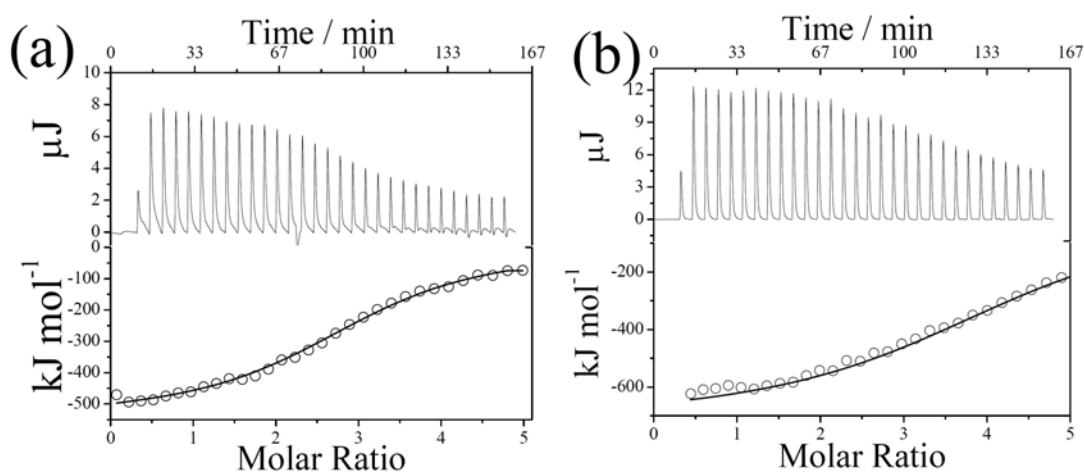


**Fig. S10.** Raw ITC data (up) and the integrated heat data with respect to time (bottom) for the interaction of the complex **1** with the CT DNA (a) and BSA (b) in 5 mM Tris-HCl/ 25 mM NaCl buffer (pH 7.2). The ITC data were corrected for the dilution of the complexes using the buffer.

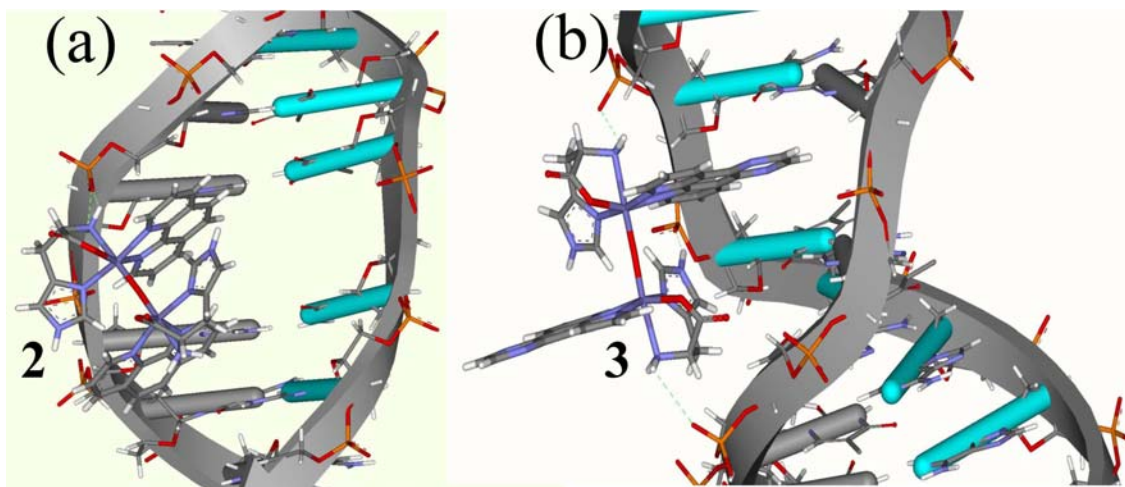
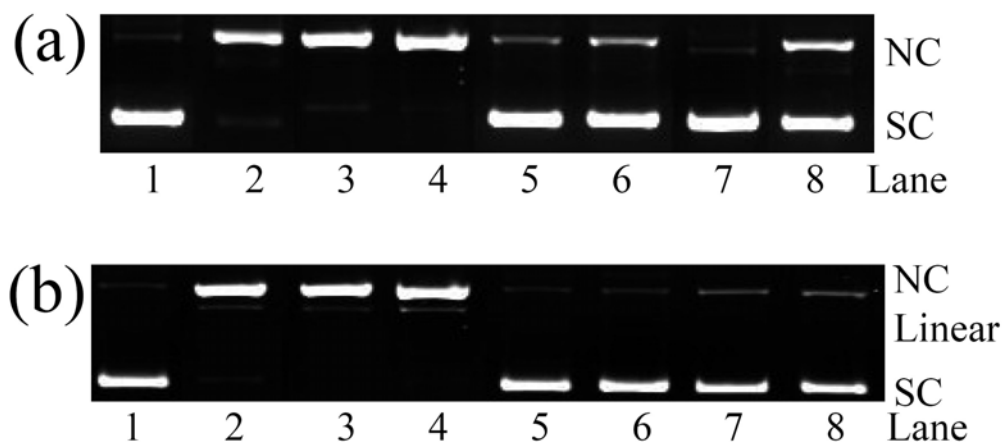


**Fig. S11.** Interaction of the complexes **2** (a) and **3** (b) with the d(CGCGAATTCGCG)<sub>2</sub> strands of DNA through hydrophobic or partial intercalation with the DNA bases.

**Molecular docking calculation:** The docking options consisted of the following steps: (i) Monte Carlo options to perform flexible fit, (ii) thresholds for diversity of saved pose (defined by user to 2Å to scan through different conformations), (iii) pose optimization that was done in two steps: (a) steepest descent minimization and (b) BFGS rigid body minimization, (iv) ligand internal energy optimization and filtering poses with short contacts (VDW and electrostatic energy calculated), and (v) pose filtering and processing with the dock scores for conformations above energy 2 kcal mol<sup>-1</sup> were accepted. Clustering of poses using leader algorithm was done. Scoring for the docked poses were determined primarily using Ludi score that considered five major contributions: (a) contributions from ideal hydrogen bonds, (b) contributions from perturbed ionic interaction, (c) contributions from lipophilic interaction, (d) contribution due to the freezing of internal degrees of freedom, and (e) contributions due to the loss of translational and rotational entropy of the ligand. A second estimate of the Ludi score was obtained by changing the weights of the above contributors, while the weights were derived from Ludi score and fitted to the experimentally determined binding affinities.



Complex + MPA (Fig.)	% NC DNA (Chemical Nuclease Activity)							
	DNA control	Complex + MPA	+ $\text{NaN}_3^a$	+ L-histidine <sup>b</sup>	+ KI <sup>c</sup>	+ DMSO <sup>d</sup>	+ Catalase <sup>e</sup>	+ SOD <sup>f</sup>
<b>2</b> + MPA (S12a)	2	88	90	92	11	19	7	29
<b>3</b> + MPA (S12b)	2	90+2	92+2	90+3	6	4	9	12

**Fig. S12.** The gel electrophoresis diagram showing the mechanistic aspects of oxidative cleavage of SC pUC19 DNA (0.2  $\mu\text{g}$ , 30  $\mu\text{M}$ ) by the complexes (**2**, **3**) in the presence of the various additives in 50 mM Tris-HCl/NaCl buffer (pH 7.2) and 3-mercaptopropionic acid (MPA) as a reducing agent. The percent of cleavage in the presence of various additives are tabulated. Complex concentration = 30  $\mu\text{M}$ . <sup>a</sup> $[\text{NaN}_3] = 500 \mu\text{M}$ . <sup>b</sup> $[\text{L-histidine}] = 500 \mu\text{M}$ . <sup>c</sup> $[\text{KI}] = 500 \mu\text{M}$ . <sup>d</sup>DMSO = 6  $\mu\text{L}$ . <sup>e</sup>Catalase = 4 units. <sup>f</sup>SOD = 4 units.

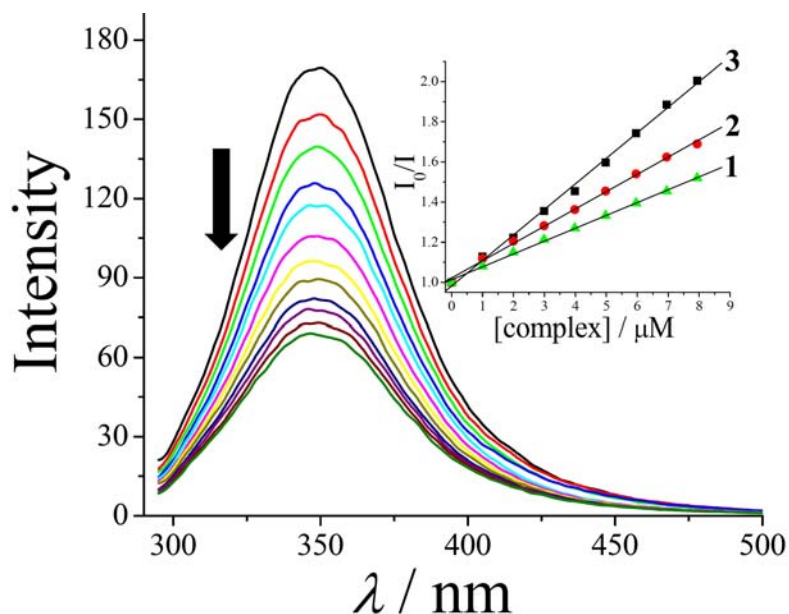


**Fig. S13.** Emission spectral traces of BSA (2  $\mu\text{M}$ ) in the presence of complex **3** with the inset showing the plot of  $(I_0/I)$  vs.  $[\text{complex}]$  for **1**(▲), **2**(●) and **3**(■).

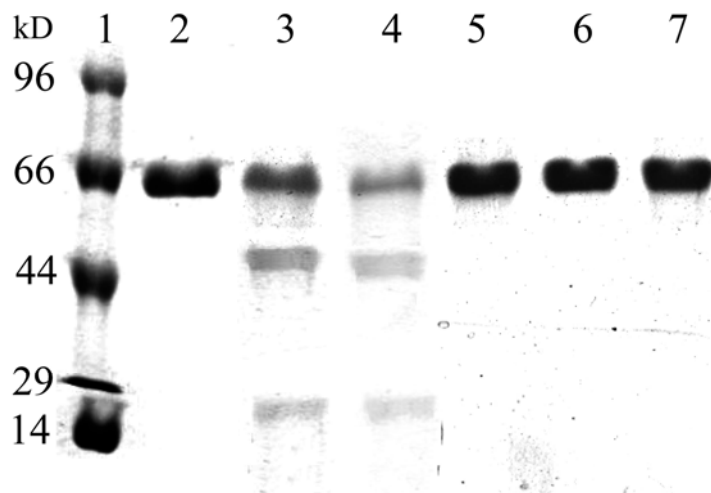


**Fig. S14.** The SDS-PAGE diagram showing the mechanistic results for the cleavage of BSA (4  $\mu\text{M}$ ) by **3** (200  $\mu\text{M}$ ) with 20 min photoexposure to UV-A light at 365 nm (100 W): lane-1, molecular marker; lane-2, BSA control; lane-3, BSA +  $\text{NaN}_3$  (3 mM) + **3**; lane-4, BSA + TEMP (3 mM) + **3**; lane-5, BSA + KI (3 mM) + **3**; lane-6, BSA + DMSO (20  $\mu\text{L}$ ) + **3**; lane-7, BSA + mannitol (3 mM) + **3**.

**Table S1.** Selected bond distances ( $\text{\AA}$ ) and bond angles ( $^\circ$ ) data for the complex  $\mathbf{1}\cdot 4\text{H}_2\text{O}$ .

Fe(1) – O(5)	1.766(12)	Fe(2) – O(5)	1.800(12)
Fe(1) – O(1)	2.046(8)	Fe(2) – O(3)	1.990(9)
Fe(1) – N(3)	2.110(12)	Fe(2) – N(8)	2.087(5)
Fe(1) – N(2)	2.160(10)	Fe(2) – N(10)	2.164(11)
Fe(1) – N(1)	2.165(10)	Fe(2) – N(6)	2.168(5)
Fe(1) – N(5)	2.227(5)	Fe(2) – N(7)	2.184(6)
O(5) – Fe(1) – O(1)	98.8(4)	O(5) – Fe(2) – O(3)	104.4(4)
O(5) – Fe(1) – N(3)	93.6(4)	O(5) – Fe(2) – N(8)	94.9(3)
O(1) – Fe(1) – N(3)	90.7(4)	O(3) – Fe(2) – N(8)	90.2(3)
O(5) – Fe(1) – N(2)	96.8(4)	O(5) – Fe(2) – N(10)	178.0(4)
O(1) – Fe(1) – N(2)	94.9(4)	O(3) – Fe(2) – N(10)	77.3(4)
N(3) – Fe(1) – N(2)	167.3(4)	N(8) – Fe(2) – N(10)	83.9(3)
O(5) – Fe(1) – N(1)	95.8(4)	O(5) – Fe(2) – N(6)	93.9(3)
O(1) – Fe(1) – N(1)	162.6(4)	O(3) – Fe(2) – N(6)	91.6(3)
N(3) – Fe(1) – N(1)	97.7(4)	N(8) – Fe(2) – N(6)	170.2(3)
N(2) – Fe(1) – N(1)	74.0(4)	N(10) – Fe(2) – N(6)	87.1(3)
O(5) – Fe(1) – N(5)	174.3(3)	O(5) – Fe(2) – N(7)	93.5(3)
O(1) – Fe(1) – N(5)	76.0(2)	O(3) – Fe(2) – N(7)	158.7(3)
N(3) – Fe(1) – N(5)	84.2(3)	N(8) – Fe(2) – N(7)	99.8(2)
N(2) – Fe(1) – N(5)	86.1(3)	N(10) – Fe(2) – N(7)	85.1(4)
N(1) – Fe(1) – N(5)	89.7(3)	N(6) – Fe(2) – N(7)	75.45(16)
Fe(1) – O(5) – Fe(2)	171.9(5)		